DOI: 10.1021/cg900465h

CRYSTAL GROWTH & DESIGN Article

2009, Vol. 9
4189–4198

Tartrate Chirality Determines Thaumatin Crystal Habit

Neer Asherie,*,† Jean Jakoncic,‡ Charles Ginsberg,† Arieh Greenbaum,† Vivian Stojanoff,‡ Bruce J. Hrnjez,§ Samuel Blass,† and Jacob Berger†

†*Department of Physics and Department of Biology, Yeshiva University, New York, New York 10033,* ‡*Brookhaven National Laboratory, National Synchrotron Light Source, Upton, New York 11973, and* §*Department of Chemistry, Yeshiva University, New York, New York 10033*

Received April 26, 2009; Revised Manuscript Received June 18, 2009

Ⓦ This paper contains enhanced objects available on the Internet at http://pubs.acs.org/crystal.

ABSTRACT: A major challenge in structural biology is to produce high-quality protein crystals for X-ray diffraction. Currently, proteins are crystallized by trial and error, often in multicomponent solutions with chiral precipitants. As proteins are chiral molecules, we hypothesized that the chirality of the precipitants may affect crystallogenesis. To test this hypothesis, we crystallized thaumatin, an intensely sweet globular protein, with the three stereoisomers (L-, D-, and *meso*-) of tartaric acid. We find three different crystal habits and crystal packings; the three stereoisomers interact with the protein at different sites. All three precipitants produce high-quality crystals from which atomic resolution (∼1 Å) structures were obtained. Our findings suggest that stereospecific interactions with precipitants are important in protein crystal formation and should be controlled when crystallizing proteins for structure determination.

Introduction

It is difficult to crystallize proteins. Fewer than 20% of purified proteins produce diffraction-quality crystals, and this "crystallization bottleneck" hampers progress in structural biology.[1] Since it is not yet possible to reliably predict the conditions under which a protein will crystallize, the main way to produce crystals is by brute-force methods: trying many different conditions in the hope that at least one of them will work.

For a solution of proteins to crystallize, the protein concentration must exceed the solubility limit, that is, the solution must be supersaturated. There are several approaches for creating supersaturated solutions, such as changing the temperature, changing the pH, or removing water by evaporation.[2] Another common approach is to add a precipitant, which can be a salt, an organic solvent, or a polymer.[3] There have been numerous investigations about the effects of precipitants on the solubility of proteins. The topics that have been studied include specific protein−ion interactions,[4,5] changes in the solution properties, such as dielectric constant,[6] and the role of the chain length of polymeric precipitants.[7]

One aspect of the protein−precipitant interactions that has not been studied extensively is the chiral nature of the molecules involved. Proteins are chiral, and a significant number of the precipitants used are also chiral. There are chiral salts (e.g., those made from tartaric acid), chiral organic solvents (e.g., 2-methyl-2,4-pentanediol, known as MPD), and chiral polymers (e.g., Jeffamine). Such chiral precipitants abound among the commercially available crystallization screens. For example, the MPD Suite manufactured by Qiagen provides a range of concentrations of MPD with either different salts or at different pH values,[8] while the Silver Bullets screen and the Tacsimate crystallization reagent manufactured by Hampton offer combinations of chiral molecules (such as the salts of tartaric and malic acids) in the same solution.[9]

Even though chiral precipitants are commonly used to crystallize proteins, little attention is paid to their chiral nature. In fact, vendors and investigators sometimes omit the stereochemical designation when describing the precipitant being used. This is puzzling for two reasons. First, without this designation the precipitant cannot be uniquely identified. Second, it is known that chirality can significantly affect the crystallization of small organic molecules. Indeed, in 1848, Pasteur discovered molecular chirality through a crystallization experiment: he found that racemic (DL-) sodium ammonium tartrate crystallized as a mixture of enantiomorphic crystals.[10] Since this pioneering work, crystal growth experiments involving small organic molecules have established the importance of chirality in these systems.[11,12] For example, racemic mixtures of amino acids can be separated by adding a suitably tailored, chiral additive which affects the crystallization of one enantiomer but not the other.[13]

As the effects of chirality on the crystallization of small molecules are dramatic, we hypothesized that the chirality of precipitants may affect the crystallization of proteins. To test this hypothesis, we sought a protein that could be crystallized with a chiral precipitant. We chose to work with thaumatin, an intensely sweet, single-domain globular protein (207 amino acids, eight disulfide bonds, molecular weight approximately 22 kDa) which is found in the fruit of *Thaumatococcus daniellii*.[14,15] Thaumatin is widely used as a model system to study various aspects of protein crystallization and crystallography.[16−22] Its popularity stems in part from the ease with which it can be crystallized using the salts of L-tartaric acid.[23] Tartaric acid has two chiral centers and three stereoisomers: L- and D-tartaric acids, which form an enantiomeric pair, and *meso*-tartaric acid, which is not chiral.[24] Thus, the thaumatin−tartrate system provides a test not only of chirality but also of the more general effects of stereoisomerism in protein crystallization.

*Corresponding author. Address: Yeshiva University, Belfer Hall 1412, 2495 Amsterdam Avenue, New York, NY 10033, USA. Phone: 212-960-5452. Fax: 212-960-0035. E-mail: asherie@yu.edu.

In a recent communication, we reported our results for the solubility of purified thaumatin crystals grown with sodium L- and D-tartrate.[25] We found that bipyramidal crystals form with L-tartrate and their solubility increases with increasing temperature; prismatic and stubby crystals form with D-tartrate and their solubility decreases with temperature. These results suggested that the two enantiomers interact differently with thaumatin. In order to confirm this suggestion and provide a molecular basis for our macroscopic observations, we report here the X-ray crystal structures of thaumatin grown with L- and D-tartrate. In addition, to address the more general question of the role of stereoisomerism, we determined the X-ray crystal structures of thaumatin grown with DL- and *meso*-tartrate. All structures were obtained to very high resolution (~1 Å), allowing the stereochemical configuration of the tartrate ions to be assigned unambiguously. We find that the three stereoisomers interact with the protein at different sites, leading to different crystal habits and crystal packings. Thus, our results provide evidence that stereospecific interactions between precipitants and proteins are important in crystallogenesis and should be controlled when crystallizing proteins.

Experimental Section

Materials. Thaumatin (batch DBDS004) was provided by Natex UK Limited, Sandy, UK. Acetic acid, sodium azide, monobasic sodium phosphate, dibasic sodium phosphate, monobasic potassium phosphate, phosphoric acid, sodium hydroxide, glycerol, and 2-propanol were purchased from Fisher Scientific, Pittsburgh, PA. L-tartaric acid (cat. no. T1807, lot no. 033K3650 and 115K3712), D-tartaric acid (cat. no. T206, lot no. 10121AD), *meso*-tartaric acid (cat. no. T3259, lot no. 107K2562), ethylene glycol, polyethylene glycol (PEG 400), and mineral oil were purchased from Sigma-Aldrich. Deionized water was obtained from an E-pure 4-Module deionization system (Barnstead International, Dubuque, IA). All materials were used without further purification, except for the thaumatin and *meso*-tartaric acid, which were purified as described below. Solutions were filtered through a Nalgene disposable 0.22 μm filter unit (Nalge Nunc International, Rochester, NY) prior to use.

Purification and Characterization of Thaumatin. Thaumatin was dissolved at about 100 mg/mL in 275 mM sodium acetate buffer (pH = 4.5, conductivity σ = 8.0 mS/cm) with 0.02% (w/v) sodium azide. The solution was centrifuged at 31000*g* for 30 min to sediment any undissolved solids. The supernatant was purified with an ÄKTAprime-plus preparatory scale low-pressure size-exclusion chromatography system (GE Healthcare, Piscataway, NJ) by isocratic elution at 1.5 mL/min on an XK26/100 column packed with Sephacryl S-200 HR resin (GE Healthcare, Piscataway, NJ). The buffer used was 275 mM sodium acetate (pH = 4.5, σ = 8.0 mS/cm) with 0.02% (w/v) sodium azide. The monomer fraction was collected and characterized as described previously.[26] These results showed that this fraction is essentially a homogeneous preparation of thaumatin I.

Purification and Characterization of *meso*-Tartaric Acid. As received, *meso*-tartaric acid has a yellow color and nutty odor. To check the purity of the *meso*-tartaric acid, reverse-phase high performance liquid chromatography (RP-HPLC) was carried out on a Beckman System Gold apparatus at a flow rate of 1 mL/min (Beckman Coulter, Fullerton, CA) by isocratic elution on a Inertsil ODS-3 V column (GL Sciences, Torrance, CA). The buffer used was 114 mM potassium phosphate buffer (pH = 2.0, σ = 8.2 mS/cm). RP-HPLC revealed that the initial *meso*-tartaric acid was contaminated by DL-tartaric acid (approximately 10%).

Meso-tartaric acid was recrystallized three times in 2-propanol. To remove small amounts of 2-propanol which remained (1−2% by number), the thrice recrystallized *meso*-tartaric acid was dissolved in water close to the solubility limit at room temperature (about 1.2 g/mL) and then placed under a vacuum to remove the solvent. The final material consisted of crystalline *meso*-tartaric acid monohydrate as confirmed by elemental analysis and ^{1}H and ^{13}C NMR measurements (data not shown). RP-HPLC showed that the purity was greater than 99.5% and the enantiomeric ratio (er) of *meso*-tartaric acid to racemic tartaric acid exceeded 99.5:0.5.

Crystallization. Purified Natex protein was dialyzed in an Amicon ultrafiltration cell with a 10 kDa membrane into 10 mM sodium phosphate buffer (pH = 7.3; σ = 1.5 mS/cm) with 0.002% (w/v) sodium azide. It was then filtered (0.22 μm) and concentrated to approximately 100 mg/mL in Centricon 10 concentrators. Though some protein precipitated during this process, the precipitate adhered to the concentrator, making it possible to collect a clear solution of protein. We found that keeping the solution on ice delayed any further precipitation while the crystallization experiment was started. Glycerol was added to the solution so that the final amount (after the addition of the precipitant) was 2.5%, 5%, or 10% (v/v).

The tartrate stereoisomer of interest (0.125 M, 0.25 M, 0.5 or 1 M solution) was prepared in 10 mM sodium phosphate buffer (pH = 7.3, adjusted with NaOH) with 0.002% (w/v) sodium azide. To prepare the racemic precipitant, equal volumes of the L-tartrate and D-tartrate precipitants were combined.

The microbatch method was used to produce crystals for X-ray diffraction studies. One microliter of precipitant was added to 1 μL of protein solution and then covered with approximately 20 μL of mineral oil in a microbatch 72-well plate (Hampton Research, Aliso Viejo, CA). Initially, both hydrophilic (cat. no. HR3-120) and hydrophobic plates (cat. no. HR3-086) were used, but after it was found that the crystals tended to stick to the hydrophilic plates, only the hydrophobic ones were used. The plates were left at a fixed temperature (typically, 4 °C or room temperature, i.e., 20 ± 2 °C) and inspected periodically by bright field microscopy with an AxioImager A1m microscope (Carl Zeiss, Gottingen, Germany). Observations were carried out for up to 2 months. Crystals were harvested with mounted cryoloops (Hampton Research, Aliso Viejo, CA) and dipped in a cryoprotectant (usually, 10−30% glycerol solution with 0.5 M of the precipitant) immediately before the diffraction measurements.

Data Collection, Refinement and Structural Analysis. All X-ray diffraction data were recorded at beamline X6A (Brookhaven National Laboratory, National Synchrotron Light Source, Upton, NY, USA) between 13.5 and 15.1 keV with the exception of the 2VI4 data that were recorded at beamline ID15A (European Synchrotron Radiation Facility, Grenoble, France) and at 56 keV. All data were recorded at 100 K using an ADSC Q210 CCD detector (Poway, CA, USA) at X6A and a MAR345 image plate (Mar Research, Norderstedt, Germany) at ID15A. Data were indexed, integrated and scaled in HKL 2000.[27] Thaumatin crystal structures were solved by molecular replacement using MOLREP[28] and the model from the PDB entry 1KWN.[16] Each model was refined by restrained maximum-likelihood refinement with REFMAC[29,30] with individual anisotropic temperature factors and manual building performed in Coot.[31] After the final refinement, stereochemistry of the structures were assessed with PROCHECK.[32] All figures were prepared with PYMOL.[33]

Results and Discussion

Crystal Habits and Crystallization Conditions. When thaumatin is crystallized with the different tartrate precipitants, we observe three crystal habits: bipyramids, prisms, and plates (Figure 1 and Table 1). With L-tartrate only bipyramids are seen (Figure 1A); these are the rapidly forming crystals which have made thaumatin a popular model system.[16−22] In contrast, when D-tartrate is used as the precipitant, prisms initially form and these grow into stubby crystals (Figure 1C). At 20 °C, this is the only type of crystal seen. However, at 4 °C bipyramids also appear after a few days (Figure 1D).

meso-Tartrate produces the same prisms and stubby crystals found with D-tartrate (Figure 1E), but no bipyramids are

observed at either 4 or 20 °C. After about 2 weeks, plates are seen to coexist with the prisms at 4 °C (Figure 1F). Plates are not observed with either L- or D-tartrate.

The addition of the racemic DL-tartrate produces a mixture of bipyramids and prisms. At 20 °C, bipyramids and many, stubby crystals coexist (Figure 1G), while at 4 °C, the bipyramids coexist with fewer, smaller prisms (Figure 1H).

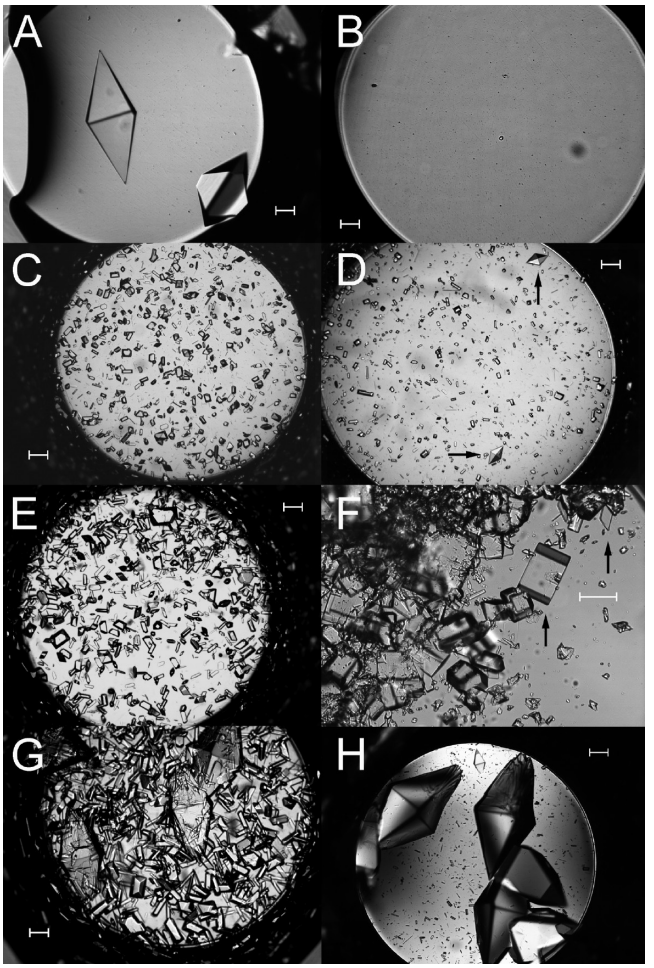

Figure 1. Crystal habits of thaumatin with the stereoisomers of tartrate. (A) Bipyramidal crystals in L-tartrate. (B) Amorphous shards in no tartrate. (C) Prisms and stubby crystals in D-tartrate. (D) Crystals in D-tartrate after 3 days; bipyramids (indicated by the arrows) have formed in addition to the prisms and stubby crystals already present. (E) Prisms and stubby crystals in *meso*-tartrate. (F) Plates (indicated by the arrows) in *meso*-tartrate after 55 days. (G) Bipyramids and stubby crystals in DL-tartrate at 20 °C. (H) Bipyramids and prisms in DL-tartrate at 4 °C. The scale bar in all figures is 100 μm.

These results are consistent with our measurements of the solubility of thaumatin grown with L- or D-tartrate.[25] At 4 °C, the bipyramids formed with L-tartrate are about 30 times less soluble than the prisms formed with D-tartrate, so most of the protein crystallizes as bipyramids. At 20 °C, the bipyramids are only 8 times less soluble than the prisms, so it is easier for prisms to form and grow into stubby crystals.

If no tartrate is added, the protein precipitates as small shards (Figure 1B). Such precipitation is also seen during the concentration of thaumatin for the crystallization experiments.[26] Shards rarely give diffraction patterns. A few diffracted reasonably well (resolution limit 1.3−1.7 Å), and they have the same crystal packing as the prisms which form in D-tartrate. Bipyramids can also form without any tartrate added, but this is a rare event and the resolution limit (1.6 Å) is much worse than when tartrate is used as a precipitant.

Overall Structure of Thaumatin. The structures of thaumatin in the different crystal habits are shown in Figure 2. Each crystal habit corresponds to a different unit cell (Tables 1 and 2, and Table S1, Supporting Information). We find tartrate molecules as part of the structures obtained from the bipyramids and the plates; no ordered tartrate is found in the prisms or stubby crystals. Tartrate, therefore, acts both as a precipitant and an additive in the formation of protein crystals.

The most studied structure of thaumatin is that obtained from bipyramids with L-tartrate (Figure 2A) because these crystals are relatively easy to produce.[23] Previous work shows that one L-tartrate molecule associates with the protein near S36 and is important in establishing crystal contacts.[16,23] We find a second L-tartrate molecule, which has not been reported previously, near K97. As we discuss below, it too connects different protein molecules in the crystal lattice.

The structure of thaumatin obtained from prisms or stubby crystals with D-tartrate (Figure 2B; red) is close to that from bipyramids formed with L-tartrate (Figure 2B; blue); the root-mean-square deviation between equivalent C_α atoms (rmsd-C_α) is around 0.59 Å (Table S2, Supporting Information). Unlike the structure obtained with L-tartrate, the one found from prisms with D-tartrate does not contain any tartrate molecules.

The protein structure determined from bipyramids which form in D-tartrate (Figure 2C; magenta) is essentially identical to that from L-tartrate (Figure 2C; blue); rmsd-C_α is 0.1 Å or less. There are, however, two significant differences between the structures: D-tartrate replaces L-tartrate at the S36 site and there is no D-tartrate at the K97 site. We note

Table 1. Crystallization Data and Conditions

Figure 1 (panel)	precipitant	habits	tartrate in crystal	temp (°C)	protein conc (mg/mL)	time elapsed	Protein Data Bank entry
A	0.25 M L-tartrate	bipyramid	L	4	44.5	24 h	2VHR; 2VHK[a]
B	none	shards	none	20	44.5	24 h	2WBZ[b]
C	0.25 M D-tartrate	prism/stubby	none	4	50.7	19 h	2VI1
D	0.25 M D-tartrate	bipyramid; prism/stubby	D; none	4	50.7	3 days	2VI2; 2VI1[c]
E	0.25 M *meso*-tartrate	prism/stubby	none	20	64.0	19 h	2VU6
F	0.25 M *meso*-tartrate	plates; prism/stubby	*meso*; none	4	40.2	55 days	2VU7; —[d]
G	0.50 M DL-tartrate	bipyramid; prism/stubby	L; none	20	50.7	19 h	2VI3; —[d]
H	0.50 M DL-tartrate	bipyramid; prism/stubby	L; none	4	50.7	19 h	2VI4; —[d]

[a] 2VHK is from bipyramids formed at 22 °C. [b] 2WBZ is from bipyramids formed at 4 °C without any tartrate after 11 days. [c] 2VI1 is from prisms formed at 22 °C; this structure is almost identical to that obtained at 4 °C. [d] The crystal packing and protein structure are almost identical to those of 2VI1 and 2VU6.

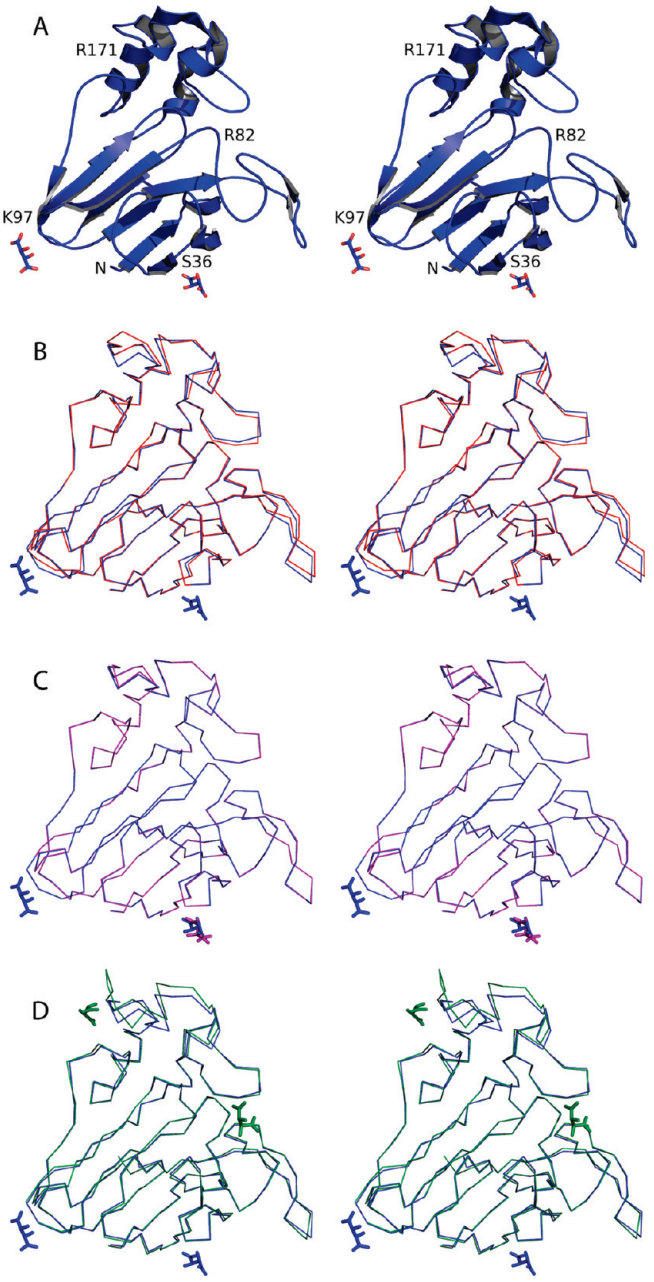

Figure 2. Overall structures of thaumatin with the stereoisomers of tartrate. (A) Stereo cartoon of thaumatin from bipyramids grown in L-tartrate (2VHK); the two L-tartrate molecules found in the structure are also shown. (B−D) Stereoview showing a superposition of the C_α atoms for thaumatin from crystals grown under different conditions. The tartrate molecules associated with each structure are also shown in the same color as the protein backbone. (B) Prisms in D-tartrate (2VI1, red) and bipyramids in L-tartrate (2VHK, blue). (C) Bipyramids in D-tartrate (2VI2, magenta) and bipyramids in L-tartrate (2VHK, blue). (D) Plates in meso-tartrate (2VU7, green) and bipyramids in L-tartrate (2VHK, blue).

that the bipyramids which grow in DL-tartrate also have no tartrate at K97, and the enantiomer near S36 is L-tartrate.

Even greater differences are seen in the structure from platy (plate-like) crystals grown in *meso*-tartrate (Figure 2D; green); rmsd-C_α from the L-tartrate structure (Figure 2D; blue) is about 0.8 Å. More importantly, the two *meso*-tartrate molecules associate with the protein at completely different sites, R82 and R171 [See movie in the HTML version of this paper showing the locations of the tartrate molecules (L-tartrate from 2VHK, D-tartrate from 2VI2, and meso-tartrate from 2VU7) in relation to the thaumatin tertiary structure (2VHK)].

We find that the overall protein structure does not change for a given crystal habit, no matter how this habit was formed. For example, rmsd-C_α is less than 0.15 Å for all bipyramids obtained under the various conditions studied. Analogously, prisms and stubby crystals obtained under different conditions also give nearly identical structures. The correspondence between habit and structure is known for other proteins which form polymorphic crystals, such as lysozyme[34] and bovine pancreatic trypsin inhibitor.[35]

Although the protein structures from a given habit are nearly identical, those from different habits are not (Table S2, Supporting Information). One important difference involves the C-terminal amino acid A207. Positive density is observed in the structures determined from prisms or plates, where A207 forms hydrogen bonds via water to neighboring protein molecules. No electron density is observed at this position in structures determined from bipyramids, presumably because such stabilizing bonds cannot form.

Tartrate Stereoisomers and Crystal Contacts. The tartrate stereoisomers dictate the crystal contacts that form. Below we examine the contacts which involve tartrate molecules in bipyramids and plates (recall that no tartrate molecules are found in prisms or stubby crystals). We observe bipyramids with L-tartrate, D-tartrate, DL-tartrate, and no tartrate (Figure 1 and Table 1); plates are observed only with *meso*-tartrate.

Bipyramids: S36 Contact Site. One important crystal contact is near S36 (Figure 2). This site has been described previously for crystals with L-tartrate,[16,23] but our 0.94 Å resolution structure provides additional details about the crystal contacts. We find that the L-tartrate molecule forms hydrogen bonds, either directly or through one water molecule, with three symmetry-related proteins involving a total of 11 protein residues: R29, G34, E35, S36, K137′, F152′, T154′, Y157′, Y169′, K67″, and P141″ (Figure 3A). Almost all of these acceptor−donor distances are shorter than 3 Å (Table S3, Supporting Information), suggesting that the hydrogen bonds are relatively strong.[36]

The conformation of the L-tartrate molecule at the S36 site is similar to that found in many salts of L- or D-tartaric acid.[37,38] That is, the four carbon atoms lie in a plane (antiplanar), the atoms comprising the carboxylate and hydroxyl groups of the same half are approximately coplanar, and the angle between the two planar halves is about 66° (Figure 4 and Table 3). Therefore, L-tartrate at the S36 site is able to provide the appropriate intermolecular contacts for crystallization while simultaneously satisfying the intramolecular constraints that determine its most stable conformation. This may explain why it is such an effective crystallizing agent for thaumatin, leading to the formation of bipyramidal crystals in a few hours and sometimes even faster.

The bipyramids produced with D-tartrate form over the course of several days, that is, much more slowly than with L-tartrate. Initially, we thought that the slower kinetics might be due to a different interaction site. We find, however, that D-tartrate occupies an almost identical location near S36 (Figure 3B). Indeed, the correspondence between the two enantiomers is almost complete: with the exception of one water molecule, every bond formed by D-tartrate has an analog with L-tartrate (Tables S3, S4 and S6, Supporting Information).

Table 2. Data Collection and Structure Refinement Statistics

PDB entry	2VHK	2VI1	2VI2	2VU7
		Data Collection		
habit	bipyramid	prism/stubby	bipyramid	plate
space group; symmetry	$P4_12_12$; tetragonal	$P2_12_12_1$; orthorhombic (1)	$P4_12_12$ tetragonal	$P2_12_12_1$; orthorhombic (2)
unit cell dimensions (Å)	$a = b = 57.88$	$a = 50.94$	$a = b = 57.91$	$a = 43.81$
	$c = 149.95$	$b = 54.30$	$c = 150.88$	$b = 63.91$
		$c = 70.81$		$c = 71.68$
resolution range (Å)	13.00−0.94	20.00−1.04	20.00−1.08	20.00−1.08
last shell	0.96−0.94	1.06−1.04	1.10−1.08	1.10−1.08
completeness[a] (%)	99.0 (100.0)	99.0 (97.7)	95.6 (70.9)	98.1 (79.2)
$I/\sigma I$[a]	31.9 (3.1)	36.1 (2.2)	56.8 (8.3)	26.3 (2.0)
R_{sym} (%)[a]	4.4 (58.9)	5.2 (70.1)	3.9 (18.3)	5.6 (33.1)
redundancy[a]	6.1 (6.7)	7.2 (6.0)	8.6 (5.0)	5.1 (2.0)
mosaicity (°)	0.15	0.24	0.18	0.43
V_M (Å^3 /Da)/solvent content (%)	2.7/54.4	2.1/41.5	2.7/54.7	2.2/43.0
		Refinement		
overall R_{cryst}/R_{free}	12.5/13.4	12.8/14.0	11.9/12.6	12.8/14.3
		Number of Atoms		
peptide chain (no. of residues)	1545 (206)	1551 (207)	1545 (206)	1551 (207)
tartrate ions[b]	20 (2; L)		10 (1; D)	20 (2; *meso*)
glycerol (no. of molecules)	18 (3)	18 (3)	18 (3)	
ethylene glycol (no. of molecules)				8 (2)
water O atoms	372	292	359	349
		Rms Deviation from Ideal		
bond length (Å)	0.010	0.012	0.011	0.015
bond angles (°)	1.552	1.560	1.524	1.727
average B factors (Å^2) (overall)	11.6	13.1	11.8	11.5
peptide main chain/side chain	8.7/10.2	10.2/12.5	9.2/10.9	8.9/10.9
tartrate ions	9.2		12.7	13.3
glycerol	13.8	11.9	13.5	
ethylene glycol				11.2
water	20.2	22.9	19.0	18.7
		Ramachandran plot		
most favored (%)	90.5	87.6	90.5	91.1
additionally favored (%)	9.5	12.4	9.5	8.9
disallowed (%)	0.0	0.0	0.0	0.0

[a] Number in parentheses refers to the highest resolution shell. [b] In parentheses: (no. of molecules in the structure; stereoisomer).

Nevertheless, the difference in the L- and D-enantiomer interactions with the protein and local water is significant. While L-tartrate adopts one stable conformation (Figure 4A), D-tartrate has two almost equally probable conformations (Figure 4B). These two conformations result from the competition between intermolecular and intramolecular interactions.

In conformer a of D-tartrate, the O1a oxygen atom of the carboxylate group is close enough to the NH1 group of R29 to make a hydrogen bond with a donor−acceptor distance of 3.11 Å (Table 3). Though this distance is greater than the corresponding bond of L-tartrate (2.90 Å), it is still within the range of lengths (2.7−3.2 Å) typically found in proteins.[39] In conformer a, however, the intramolecular hydrogen bonding between O1a and the neighboring hydroxyl oxygen O3 is not optimal. The torsion angle of atoms O1a−C1−C2−O3 is −49.4°; the carboxylate and hydroxyl groups are far from being coplanar. In contrast, the corresponding torsion angle in L-tartrate is 16.4°, which is within the range observed in L- or D-tartrate crystals (−20° to +20°).

In conformer b, the O1b−C1−C2−O3 torsion angle is 1.3° and the O1b−O3 distance is 2.62 Å suggesting intramolecular hydrogen bonding. However, the carboxylate oxygen is so far from the NH1 group of R29 (3.99 Å) that an intermolecular hydrogen bond can no longer form.

The suboptimal nature of the D-tartrate configuration is apparent also from the interaction between the other hydroxyl atom O4 and the NH2 group of R29. In order to form this hydrogen bond (donor−acceptor length 2.85 Å), the O4−C3−C4−O5 torsion angle of −28.5° must exceed the optimal limit. For L-tartrate, the corresponding hydrogen bond can form (the length of O3−NH2 is 2.88 Å) and still maintain the near-coplanarity of the hydroxyl and carboxylate groups (O1−C1−C2−O3 torsion angle 16.4°).

Thus, while there is a correspondence between the bonds that L- or D-tartrate can form with the proteins, D-tartrate cannot satisfy both the intermolecular and intramolecular bonding constraints as well as L-tartrate can. That is, D-tartrate binds to this site with a lower probability. This is the likely reason for the slower crystallization of bipyramids with D-tartrate.

The experiments with racemic (DL)-tartrate support our view that L-tartrate is better suited than D-tartrate for the S36 binding site. The bipyramids which form with the racemate always contain L-tartrate at this binding site (Table S1, Supporting Information).

The results also suggest that R29 is a particularly important residue for crystallization. This is confirmed by our experiments without tartrate. If no tartrate is added to the solution, bipyramids form only rarely and they are much smaller ($< 50\,\mu$m) than those seen with L- or D-tartrate. In one case, we were able to determine the protein structure at 1.6 Å (2WBZ, Table S1, Supporting Information). There are four water molecules which replace four oxygen

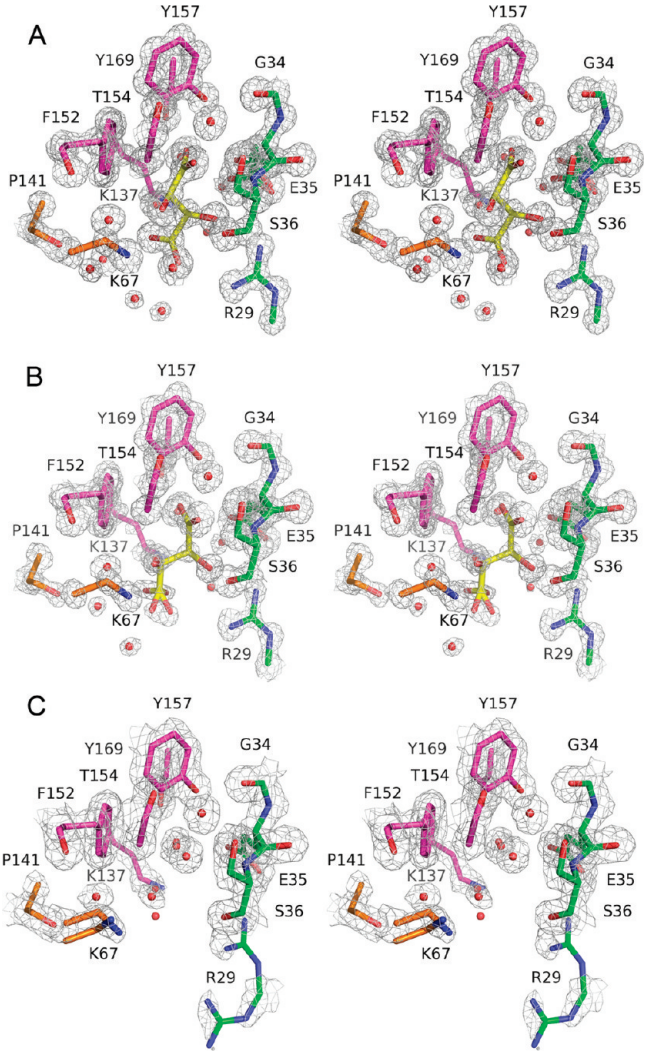

Figure 3. Crystal contact site of L- and D-tartrate in bipyramidal crystals. Stereoview of the crystal contact site near S36. (A) L-tartrate (2VHK); (B) D-tartrate (2VI2); and (C) no tartrate (2WBZ). The tartrate molecule (yellow) interacts with three symmetry-related proteins (shown with green, magenta, and orange carbon atoms) through a network of hydrogen bonds, which are either direct bonds or via water (O atoms shown as red spheres). The $2F_o - F_c$ density for this and other figures is shown as a gray mesh, contoured at 1.5σ.

atoms of the missing L- or D-tartrate molecule. These water molecules allow for some of the intermolecular hydrogen bonds found with tartrate to form (Tables S5 and S6, Supporting Information). Although many hydrogen bonds are lost without L- or D-tartrate, most of the protein residues are at positions similar to those found with tartrate. R29, however, is a notable exception (Figure 3C). It occupies with equal probability two conformations where the terminal carbon atoms are about 4.1 Å apart, and it is not involved in any intermolecular hydrogen bonding through water. It is likely that fewer hydrogen bonds and the consequent floppiness of R29 are the reasons why the formation of a bipyramid without tartrate is such a rare event.

Bipyramids: K97 Contact Site. The bipyramids grown in L-tartrate contain a second tartrate molecule near K97 (Figure 2) which is involved in making crystal contacts. It forms hydrogen bonds, either directly or through one water

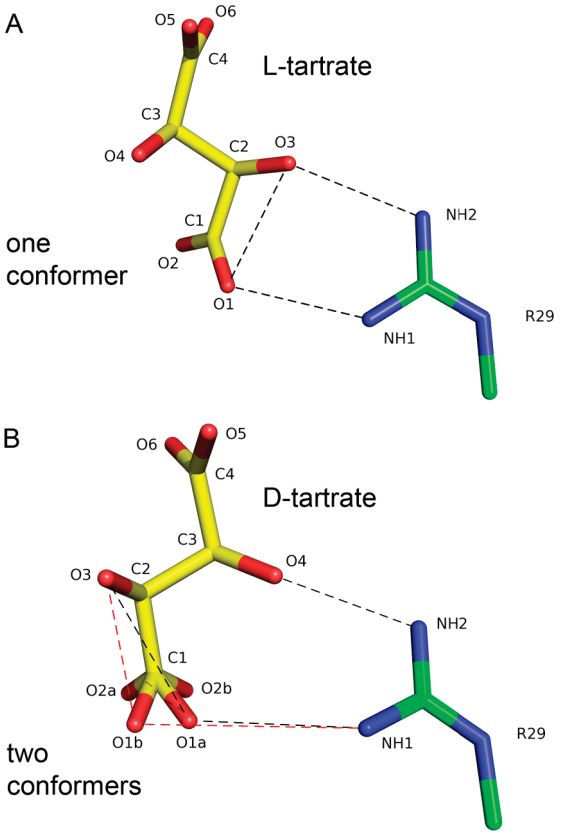

Figure 4. Selected hydrogen bonds at the crystal contact site of L- and D-tartrate in bipyramids. (A) L-Tartrate (2VHK) and (B) D-tartrate (2VI2) interacting with R29. The dashed red and black lines denote the bonds for the two conformers of D-tartrate (conformer a in black; conformer b in red).

Table 3. Atomic Distances and Torsion Angles for L- and D-Tartrate at the Bipyramidal Contact Site

L-tartrate (2VHK)		D-tartrate (2VI2)	
atoms[a]	distance (Å)[b]	atoms	distance (Å)
O1−NH1	2.90	O1a−NH1	3.11
		O1b−NH2	3.99
O1−O3	2.72	O1a−O3	2.91
		O1b−O3	2.62
O3−NH2	2.88	O4−NH2	2.85
O4−O5	2.57	O4−O5	2.71
		O4−O1a	2.93
atoms	torsion (°)	atoms	torsion (°)
C1−C2−C3−C4	−178.2	C1−C2−C3−C4	177.9
O1−C1−C2−O3	16.4	O1a−C1−C2−O3	−49.4
		O1b−C1−C2−O3	1.3
O3−C2−C3−O4	−64.8	O3−C2−C3−O4	65.3
O4−C3−C4−O5	14.0	O4−C3−C4−O5	−28.5

[a] The symbols used refer to the atoms shown in Figure 4. [b] The distances are between non-hydrogen nuclei.

molecule, with two symmetry-related proteins involving a total of six protein residues: G96, K97, G195, S196, A136′, and K137′ (Figure 5). Also, this L-tartrate molecule, like the one near S36, adopts the commonly observed L-tartrate conformation: the four carbon atoms lie in a plane, the carboxylate and hydroxyl groups of the same half are approximately coplanar, and the angle between the two planar halves is about 66°.

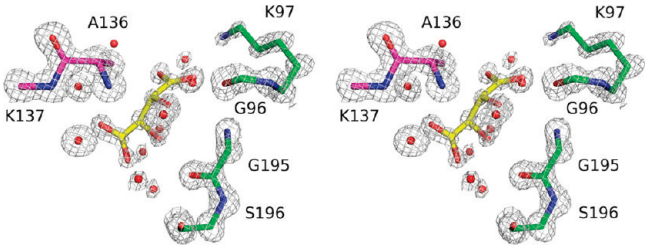

Figure 5. Stereoview of the L-tartrate crystal contact site near K97 for bipyramids (2VHK). The L-tartrate molecule (yellow) interacts with two symmetry-related proteins (shown with green and magenta carbon atoms).

Although the L-tartrate near K97 adopts a favorable conformation, the binding is not as strong as at the S36 site. The electron density of the K97 L-tartrate is not as well-defined and the occupancy is only 0.50 (vs 1.00 for the S36 L-tartrate). Furthermore, we observe this L-tartrate molecule only in experiments where pure L-tartrate is the precipitant. It is absent in experiments with precipitants DL-tartrate or D-tartrate, suggesting that binding occurs at this site only when the concentration of free L-tartrate is sufficiently high. This may be a consequence of the fewer intermolecular hydrogen bonds which are made at this site.

Our best structures—those with highest resolution and lowest mosaicity—are the ones obtained from crystals grown in pure L-tartrate (Tables 2 and S1, Supporting Information). It is likely that the additional crystal contact site at K97 contributes to the rigidity of the protein resulting in improved diffraction, but further work must be carried out to confirm this hypothesis.

Plates: R171 and R82 Contact Sites. Plates are formed when *meso*-tartrate is used as the precipitant. There are two contact sites involving *meso*-tartrate in these crystals; one is near R171 and the other is near R82 (Figure 2). At both sites, the *meso*-tartrate forms hydrogen bonds, either directly or through one water molecule, with two symmetry-related proteins (Figure 6). At the R171 site, the contact involves seven protein residues: R171, R175, D25′, G28′, R29′, W37′ and R76′ (Figure 6A); at the R82 site, eight residues are involved: D70, G72, R79, F80, G81, R82, Q153′ and S155′ (Figure 6B; T154′ is shown for completeness).

Unlike L-tartrate, the conformation of *meso*-tartrate at each contact site is different: the two *meso*-tartrate molecules are essentially mirror images of each other (the C1−C2−C3−C4 torsion angle for the *meso*-tartrate at R171 is −79.4°, while it is 71.1° for the *meso*-tartrate at R82). These conformations are different from those of L- and D-tartrate, where the four carbon atoms are coplanar.[40] The variability in the conformation of *meso*-tartrate is consistent with what is found in the salts of *meso*-tartaric acid, where the conformation of the *meso*-tartrate depends on the cations with which it crystallizes.[41−43] In our case, each chiral protein site selects for one of two enantiomeric conformers of the achiral *meso*-tartarte.

The *meso*-tartrate contact sites are rich in arginine residues. Indeed, as we observed with R29 at the bipyramidal crystal contact site (Figure 3), all arginines at the two *meso*-tartrate contact sites adopt conformations which allow direct or indirect hydrogen bonding with *meso*-tartrate. Furthermore, these conformations promote crystal contacts not mediated directly by the *meso*-tartrate such as a hydrogen bond between R79 and Q153 (Figure 6B). The importance of the interaction

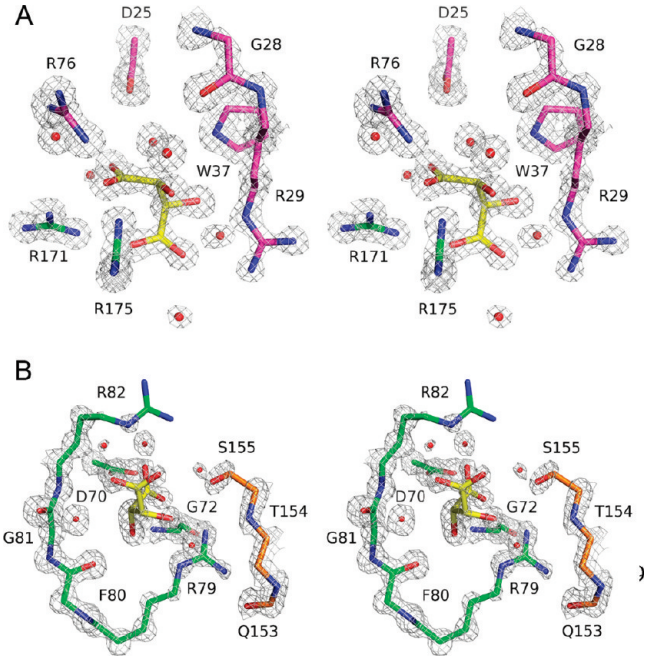

Figure 6. Crystal contact sites of *meso*-tartrate in plates. (A) Stereoview of the *meso*-tartrate crystal contact site near R171. The *meso*-tartrate molecule (yellow) interacts with two symmetry-related proteins (shown with green and magenta carbon atoms) in the platy crystals (2VU7). (B) Stereoview of the *meso*-tartrate crystal contact site near R82. The *meso*-tartrate molecule interacts with two symmetry-related proteins (shown with green and orange carbon atoms).

between *meso*-tartrate and the arginine residues is confirmed by examining a similar crystal packing of thaumatin (i.e., same unit cell) which was obtained at lower resolution (1.75 Å) without the use of tartrate (PDB ID: 1THV).[23] None of the six arginines in this structure are at the same locations as in our structures with *meso*-tartrate; the distance between the terminal carbon atoms of equivalent arginine residues are in the range 0.96 Å (R29) to 5.48 Å (R171).

Crystal Packing. The crystal packings of the bipyramids with L-tartrate and the plates with *meso*-tartrate are shown in Figure 7. As discussed above, there are two L-tartrate molecules in the bipyramidal structure (Figure 7A): one molecule near S36 (Figure 3A) connects three symmetry-related proteins (tartrate shown in red), and the other near K97 (Figure 5) connects two proteins (tartrate shown in blue). The plates also contain two tartrate molecules (Figure 7B), but each *meso*-tartrate connects only two proteins; the tartrate near R171 (Figure 6A) is shown in red, and the one near R82 (Figure 6B) is shown in blue.

The packing of the prisms which we find with precipitants D- and *meso*-tartrate does not involve any tartrate molecules. The prisms grown in D-tartrate have a different solubility than the bipyramids grown in L-tartrate: the solubility of the prismatic crystals decreases with increasing temperature, while the solubility of the bipyramids increases with temperature.[25] This difference may be connected to the presence or absence of tartrate in the crystal, and we are currently conducting further solubility measurements to test this hypothesis.

Role of Additives. The principal additive we used to obtain the high-resolution structures is glycerol. In our experiments, glycerol has two roles. First, it increases the viscosity of the crystallization solution, slowing the diffusion of protein

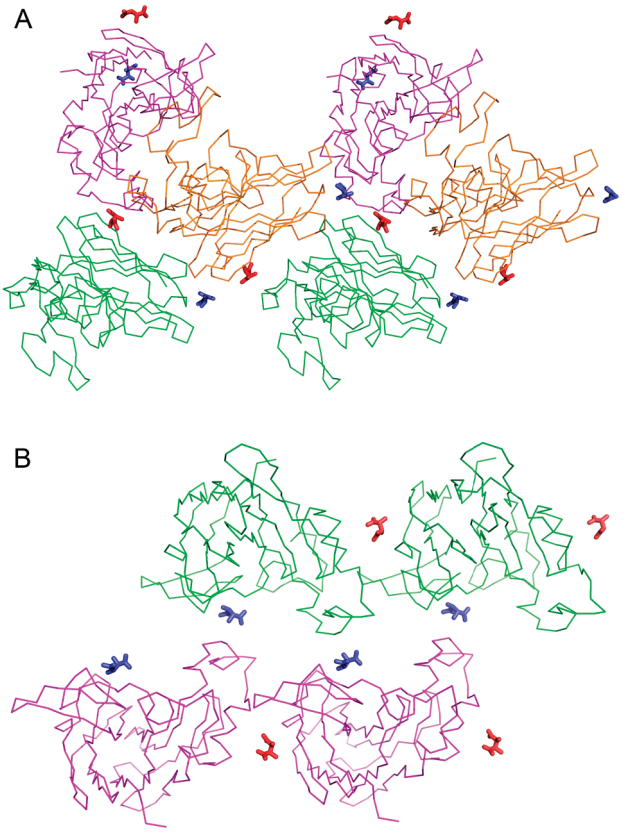

Figure 7. Packing of thaumatin molecules with crystal contacts mediated by tartrate ions. (A) Bipyramidal crystals (2VHK) where one L-tartrate (red) interacts with three protein molecules and the other L-tartrate (blue) interacts with two protein molecules. (B) Platy crystals (2VU7) where each of the two *meso*-tartrate molecules (red and blue) interacts with two protein molecules.

molecules. As a result, the nucleation and growth of the crystals are altered so that fewer and larger crystals are formed. Second, glycerol acts as a cryoprotectant. Without glycerol, the highest resolution we could obtain was 1.3 Å, and it was usually much lower. With glycerol, we obtained many data sets with a resolution better than 1 Å.

The glycerol molecules associate with the protein. Three glycerols per protein are found in both the bipyramids formed in L-tartrate (Figure S1A, Supporting Information) and the prisms formed in D-tartrate (Figure S1B, Supporting Information), but the glycerol occupies different locations in the two habits.

The plates formed in *meso*-tartrate were grown in glycerol, but we discovered that glycerol was not an optimal cryoprotectant for these crystals. Therefore, we used 35% (v/v) ethylene glycol; we find two molecules of ethylene glycol per protein in these crystals (Figure S1C, Supporting Information).

Our results with the plates suggested that the additives diffuse into the crystal lattice from the cryoprotectant and do not participate in the crystal nucleation and growth. To confirm this suggestion, we performed two sets of experiments. In the first, we took small, prismatic crystals grown with glycerol (but without tartrate) and used 30% (v/v) of ethylene glycol as the cryoprotectant instead of glycerol. In the second, we took crystalline shards of thaumatin which formed without glycerol and used two cryoprotectants, each at 30% (v/v): glycerol and ethylene glycol. In all experiments, the additive we found in the structures was the one used in the cryoprotectant. Another experiment, in which polyethylene glycol (PEG 400) was used as the cryoprotectant for prisms grown without glycerol, revealed no additive in the structure. It is possible that the PEG does not diffuse into the crystal. Alternatively, the PEG may be disordered in the lattice and thus is not seen in the electron density maps.

The resolution of the structure must be fairly high for additives to be observed. We could not confidently identify any glycerol molecules in the lower resolution (1.6 Å) bipyramids grown without tartrate (2WBZ, Table S1, Supporting Information) when glycerol was the cryoprotectant. This is consistent with previous observations.[44] Even though glycerol was used as a cryoprotectant, it was not observed in the X-ray structure; its presence was deduced from the displacement of water molecules.

Finally, we confirmed that the tartrate molecules are an integral part of crystal formation and do not diffuse into the crystal at a later stage. Prisms formed without tartrate do not incorporate D-tartrate into their structure when soaked briefly in a 500 mM solution of D-tartrate.

Thaumatin as a Sweet, Model Protein. Interest in the structure of thaumatin has persisted since the protein was first crystallized over 30 years ago.[45] Thaumatin has been crystallized in five different habits with a variety of precipitants and under many different conditions, including crystallization in gel and in microgravity.[16,46−48] There are two factors which drive this interest: a desire to understand the unusual sweetness of the protein—about 100 000 times sweeter than sucrose on a molar basis[49]—and the use of thaumatin as a model protein in crystallization and crystallography studies.

The structural basis for the intense sweetness of thaumatin is still incomplete. There is no sequence homology between thaumatin and other sweet proteins, and the binding mechanism of thaumatin is not fully understood.[50] Mutational studies identified numerous residues which affect the sweetness of the protein. It was recently shown that K67 and R82 are critical residues in eliciting the sweetness response.[51] The two residues are close (the distance between the C_α atoms is less than 9 Å) suggesting that the sweet taste receptor recognizes this region of the protein. Since these residues are at the sites where L-tartrate and *meso*-tartrate interact with the protein, it should be possible to alter the sweetness and bitter aftertaste of thaumatin by adding suitable small molecules.

It has been noted that local, rather than global, structural changes determine the sweetness of thaumatin.[51] Thus, it is important to work with structures that provide sufficient detail when investigating thaumatin's sweetness. Our high-resolution structures are therefore starting points for experimental and computational studies of thaumatin's sweetness.

Although thaumatin is used frequently as a model protein, few of the available structures are of high quality. Some are more than a decade old and are understandably at lower resolution. For most structures, however, there is an inconsistent assignment of residues; the amino acid sequence reported does not correspond to the known cDNA sequence of thaumatin I.[52] This is due in part to low resolution, but also results from using impure protein.

Most investigators use the unpurified thaumatin from Sigma-Aldrich which is a 3:1 mixture (molar ratio) of thaumatin I and II.[26] Thaumatin II differs from thaumatin I at five positions: N46K, S63R, K67R, R76Q, N113D.[52] We

would expect that if the unpurified protein is used, the electron density at some or all of these positions should be noisy. This is indeed the case for two previously reported tetragonal packings of thaumatin: 1KWN[16] at 1.2 Å and 1RQW at 1.05 Å (Ma et al., to be published). The sequence of thaumatin I is assigned to the protein for 1KWN, while the sequence chosen for 1RQW does not correspond to any known thaumatin sequence. In our experiments, we use purified thaumatin I and our X-ray structures are consistent with the amino acid sequence of the protein.

We have been able to establish the usefulness of using stereochemically pure precipitants by working with pure protein. For example, we crystallized thaumatin in three of its five known habits simply by changing the stereoisomer of tartrate used as a precipitant; the structure we obtained for each habit is at a much higher resolution than has been found before. Furthermore, the use of stereochemically pure precipitants reveals interactions not seen in earlier studies, such as the second L-tartrate near K97 (Figure 5). We believe that this crystal contact was not observed previously because of either low resolution[23] or the use of racemic tartrate.[16]

Our findings are consonant with recent results showing how small organic molecules can be used to crystallize proteins, often by making stabilizing crystal contacts.[53] However, these experiments typically involve cocktails of many small molecules as the precipitant; our work suggests that high-resolution structures are most likely to be obtained when the precipitant is stereochemically pure. The prisms which we grow in D- or *meso*-tartrate diffract to 0.95 Å; those grown in a cocktail without tartrate diffract to 1.6 Å.

Finally, our work shows that controlling precipitant stereochemistry can be helpful when crystallizing protein. It is therefore disheartening to see inconsistencies in the stereochemical designation of molecules in the Protein Data Bank. Sometimes these problems are minor. An incorrect identifier name can cause confusion when a racemic precipitant is used (e.g., the L-tartrate in 1KWN is labeled as D-tartrate in the "ligand chemical component").[16] In other cases, the problem is more serious, such as when impossible stereochemical assignments are made (e.g., the precipitate used in 2C1L is L-tartrate, but the PDB entry contains also D- and *meso*-tartrate).[54] These findings should encourage others to carefully consider the role of precipitant stereochemistry when crystallizing proteins.

Conclusions

We report here atomic resolution structures of thaumatin that demonstrate the benefits of using pure protein and stereochemically pure precipitants for crystallizing proteins. Our findings provide the basis for biophysical studies into the mechanism by which the stereochemistry of precipitants changes the thermodynamics and kinetics of protein crystallization. We expect that the structures we have determined will be useful for understanding the unusual sweetness of thaumatin.

Acknowledgment. We are grateful to Alessandra Polara for valuable advice and for conducting the NMR experiments. We thank Paola Dozzo, Jianfeng Jiang, George Thurston, and Jerome Karp for helpful discussions. We also thank Charles Boy of Natex UK Limited for generously providing the thaumatin used in this work. Financial support was provided by Yeshiva University (to N.A.), the Milton and Miriam Handler Foundation (to N.A.), the Kressel Scholars Program (to N.A. and S.B.), and the National Science Foundation (to N.A.; DMR 0901260). We thank the staff of the National Synchrotron Light Source, Brookhaven National Laboratory for their continuous support. The NSLS is supported by the U.S. Department of Energy, Office of Basic Energy Sciences, under contract no. DE-AC02-98CH10886. The NIGMS East Coast Structural Biology Facility, the X6A beamline, is funded under contract no. GM-0080.

Supporting Information Available: A table of the data collection and refinement statistics for PDB entries 2VHR, 2VI3, 2VI4, 2VU6, and 2WBZ; a table of the root-mean-square deviation between equivalent C_α atoms for all nine PDB entries; four tables of the atomic distances and equivalent bonds at the S36 site in bipyramidal crystals; and a stereoview of the locations of the additives used in relation to protein structures (2VHK, 2VI1, 2VU7). This material is available free of charge via the Internet at http://pubs.acs.org. Coordinates and structure factors have been deposited in the Protein Data Bank (http://www.rcsb.org/) with accession numbers 2VHK, 2VHR, 2VI1, 2V12, 2VI3, 2VI4, 2VU6, 2VU7, and 2WBZ.

References

(1) Chayen, N. E.; Saridakis, E. *Nat. Methods* **2008**, *5*, 147–153.
(2) McPherson, A. *Crystallization of Biological Macromolecules*; Cold Spring Harbor Laboratory Press: Cold Spring Harbor, NY, 1999.
(3) Dumetz, A. C.; Chockla, A. M.; Kaler, E. W.; Lenhoff, A. M. *Cryst. Growth Des.* **2009**, *9*, 682–691.
(4) Riès-Kautt, M. M.; Ducruix, A. F. *J. Biol. Chem.* **1989**, *264*, 745–748.
(5) Annunziata, O.; Payne, A.; Wang, Y. *J. Am. Chem. Soc.* **2008**, *130*, 13347–13352.
(6) Sedgwick, H.; Cameron, J. E.; Poon, W. C. K.; Egelhaaf, S. U. *J. Chem. Phys.* **2007**, *127*, 125102.
(7) Bončina, M.; Reščič, J.; Vlachy, V. *Biophys. J.* **2008**, *95*, 1285–1294.
(8) The detailed composition of the MPD Suite is available at http://www1.qiagen.com/Products/Protein/Crystallization/ScreensAnalyzingSinglePrecipitantTypes/MPDSuite.aspx.
(9) More details are available at http://hamptonresearch.com/product_detail.aspx?cid=1&sid=179&pid=562.
(10) Gal, J. *Chirality* **2008**, *20*, 5–19.
(11) Parschau, M.; Romer, S.; Ernst, K.-H. *J. Am. Chem. Soc.* **2004**, *126*, 15398–15399.
(12) Noorduin, W. L.; Izumi, T.; Millemaggi, A.; Leeman, M.; Meekes, H.; Van Enckevort, W. J. P.; Kellogg, R. M.; Kaptein, B.; Vlieg, E.; Blackmond, D. G. *J. Am. Chem. Soc.* **2008**, *130*, 1158–1159.
(13) Addidi, L.; Berkovitch-Yellin, Z.; Domb, N.; Gati, E.; Lahav, M.; Leiserowitz, L. *Nature* **1982**, *296*, 21–26.
(14) van der Wel, H.; Loeve, K. *Eur. J. Biochem.* **1972**, *31*, 221–225.
(15) Kim, S.-H.; Weickman, J. L. In *Thaumatin*; Witty, M.; Higginbotham, J. D., Eds.; CRC Press: Boca Raton, 1994; Chapter 10, pp 135−150.
(16) Sauter, C.; Lorber, B.; Giegé, R. *Proteins* **2002**, *48*, 146–150.
(17) Nanao, M. H.; Sheldrick, G. M.; Ravelli, R. B. G. *Acta Crystallogr. D* **2005**, *61*, 1227–1237.
(18) Chen, D. L.; Gerdts, C. J.; Ismagilov, R. F. *J. Am. Chem. Soc.* **2005**, *127*, 9672–9673.
(19) Lau, B. T. C.; Baitz, C. A.; Dong, X. P.; Hansen, C. L. *J. Am. Chem. Soc.* **2007**, *129*, 454–455.
(20) Kim, C. U.; Hao, Q.; Gruner, S. M. *Acta Crystallogr. D* **2007**, *63*, 653–659.
(21) Wang, L.; Lee, M. H.; Barton, J.; Hughes, L.; Odom, T. W. *J. Am. Chem. Soc.* **2008**, *130*, 2142–2143.
(22) Teixeira, S. C. M.; Blakeley, M. P.; Leal, R. M. F.; Mitchell, E. P.; Forsyth, V. T. *Acta Crystallogr. F* **2008**, *64*, 378–381.
(23) Ko, T.-P.; Day, J.; Greenwood, A.; McPherson, A. *Acta Crystallogr. D.* **1994**, *50*, 813–825.
(24) Derewenda, Z. S. *Acta Crystallogr. D* **2008**, *64*, 246–258.
(25) Asherie, N.; Ginsberg, C.; Blass, S.; Greenbaum, A.; Knafo, S. *Cryst. Growth Des.* **2008**, *8*, 1815–1817.
(26) Asherie, N.; Ginsberg, C.; Greenbaum, A.; Blass, S.; Knafo, S. *Cryst. Growth Des.* **2008**, *8*, 4200–4207.
(27) Otwinowski, Z.; Minor, W. *Methods Enzymol.* **1997**, *276*, 307–326.
(28) Vagin, A.; Teplyakov, A. *J. Appl. Crystallogr.* **1997**, *30*, 1022–1025.

(29) Murshudov, G. N.; Vagin, A. A.; Dodson, E. J. *Acta Crystallogr. D* **1997**, *53*, 240–255.
(30) CCP4—Collaborative Computational Project, Number 4; *Acta Crystallogr. D* 1994, *50*, 760-763
(31) Emsley, P.; Cowtan, K. *Acta Crystallogr. D* **2004**, *60*, 2126–2132.
(32) Laskowski, R. A.; MacArthur, M. W.; Moss, D. S.; Thornton, J. M. *J. Appl. Crystallogr. 26* **1993**, 283–291.
(33) DeLano, W. L. The PyMOL Molecular Graphics System; DeLano Scientific, LLC: SanCarlos, CA, 2006.
(34) Vaney, M. C.; Broutin, I.; Retailleau, P.; Douangamath, A.; Lafont, S.; Hamiaux, C.; Prange, T.; Ducruix, A.; Riès-Kautt, M. *Acta Crystallogr. D* **2001**, *57*, 929–940.
(35) Hamiaux, C.; Pérez, J.; Prangé, T.; Veesler, S.; Riès-Kautt, M.; Vachette, P. *J. Mol. Biol.* **2000**, *297*, 697–712.
(36) Langkilde, A.; Kristensen, S. M.; Lo Leggio, L.; Mølgaard, A.; Jensen, J. H.; Houk, A. R.; Poulsen, J-C. N.; Kauppinen, S.; Larsen, S. *Acta Crystallogr. D* **2008**, *64*, 851–863.
(37) Gorbitz, C. H.; Sagstuen, E. *Acta Crystallogr. E* **2008**, *64*, m507–m508.
(38) Ambday, G. K.; Kartha, G. *Acta Crystallogr. B* **1968**, *24*, 1540–1547.
(39) Cheung, J.; Hendrickson, W. A. *Structure* **2009**, *17*, 190–201.
(40) Stouten, P. F. W.; Kroon-Batenburg, L. M. J.; Kroon, J. *J. Mol. Struct. (Theochem)* **1989**, *200*, 169–187.
(41) De Vries, A. J.; Kroon, J. *Acta Crystallogr. C* **1984**, *40*, 1542–1544.
(42) Blankensteyn, A. J. A. R.; Kroon, J. *Acta Crystallogr. C* **1985**, *41*, 182–184.
(43) Kroon, J.; Peerdeman, A. F.; Bijvoet, J. M. *Acta Crystallogr.* **1965**, *19*, 293–297.
(44) Charron, C.; Kadri, A.; Robert, M.-C.; Giegé, R.; Lorber, B. *Acta Crystallogr. D* **2002**, *58*, 2060–2065.
(45) van der Wel, H.; van Soest, T. C.; Royers, E. C. *FEBS Lett.* **1975**, *56*, 316–317.
(46) Ogata, C. M.; Gordon, P. F.; de Vos, A. M.; Kim, S.-H. *J. Mol. Biol.* **1992**, *228*, 893–908.
(47) Lorber, B.; Ng, J. D.; Lautenschlager, P.; Giegé, R. *J. Cryst. Growth* **2000**, *208*, 665–677.
(48) Charron, C.; Giegé, R.; Lorber, B. *Acta Crystallogr. D* **2004**, *60*, 83–89.
(49) Higginbotham, J. D. In *Developments in Sweeteners*; Hough, C. A. M., Parker, K. J., Vlitos, A. J., Eds.; Applied Science Publishers: London, 1979; Vol. 1, Chapter 4, pp 87—123.
(50) Temussi, P. A. *J. Mol. Recognit.* **2006**, *19*, 188–199.
(51) Ohta, K.; Masuda, T.; Ide, N.; Kitabatake, N. *FEBS J.* **2008**, *275*, 3644–3652.
(52) Edens, L.; Heslinga, L.; Klok, R.; Ledeboer, A. M.; Maat, J.; Toonen, M. Y.; Visser, C.; Verrips, C. T. *Gene* **1982**, *18*, 1–12.
(53) Larson, S. B.; Day, J. S.; Nguyen, C.; Cudney, R.; McPherson, A. *Cryst. Growth Des.* **2008**, *8*, 3038–3052.
(54) Grazulis, S.; Manakova, E.; Roessle, M.; Bochtler, M.; Tamulaitiene, G.; Huber, R.; Siksnys, V. *Proc. Natl. Acad. Sci. U.S.A.* **2005**, *102*, 15797–15802.